V European Conference on Computational Fluid Dynamics
ECCOMAS CFD 2010
J. C. F. Pereira and A. Sequeira (Eds)
Lisbon, Portugal,14-17 June 2010

CFD OF AIR FLOW IN HYDRO POWER GENERATORS FOR CONVECTIVE COOLING, USING OPENFOAM

Pirooz Moradnia, Håkan Nilsson

Chalmers University of Technology
412 96 Gothenburg, Sweden
e-mail: {pirooz.moradnia,hakan.nilsson}@chalmers.se

Key words: CFD, Generator, Cooling, OpenFOAM, Launder-Sharma k-ε

Abstract. *The air flow field in a simplified hydro power generator has been investigated numerically with the help of OpenFOAM. Different designs of the rotor and stator have been considered and the results are compared to each other. The results show that the addition of thin baffles significantly improve the total flow, and the flow distribution through the machine. The addition of radial fan blades further improve the air flow. The simulations are based on the Frozen Rotor approach, where the rotor mesh is fixed with respect to the stator mesh, and rotational source terms are added to the equations in the rotor region. The simulations are steady-state, and the low-Re Launder-Sharma turbulence model is used. The total volume flow is predicted by the solution by including a recirculation region and avoiding inlets and outlets, thus avoiding a prescription of the volume flow. Two simple validation test cases have also been used for validation, a backward facing step and the laminar flow between concentric cylinders. Those cases have flow features that are important for the air flow in hydro power generators. The numerical results are in good agreement with theory and experiments.*

1 INTRODUCTION

Hydroelectric power generation plays an important role in the total electric power generation in Sweden. Almost half of the electric power in Sweden is generated by hydroelectric power plants and any modifications and improvements of the system would lead to a significant contribution to the total electric energy production. Two large sources of losses in the electric generators are the thermal and ventilation losses. The electric resistance in the generator system causes heat generation in windings and coils, which decreases the total efficiency of the stator in delivering power and causes thermal stresses in components. The generators are thus cooled by air flowing through the rotor and stator.

This paper focuses on generators cooled by axial air flow. The name axial suggests that the air flow in the space between rotor the and stator is along the axis of rotation. It is important to have a good understanding of the complicated flow field in the air passages in the generator in order to be able to make improvements to the design of the cooling of the system. The air flow is partially driven by the rotation of the rotor and its appended poles, which will act as a fan, into the radially extended stator channels. Radial fans are added to increase the air flow further. The air thus cools the stator body and the stator coils.

2 CASE DESCRIPTION AND MODELING

A generator can be broken down into two main parts, a rotor and a stator. Figure 1 shows the rotor and stator used in the present work. This is a simplified model of a research unit that will be used for experimental validation of the methodology used in the present work.

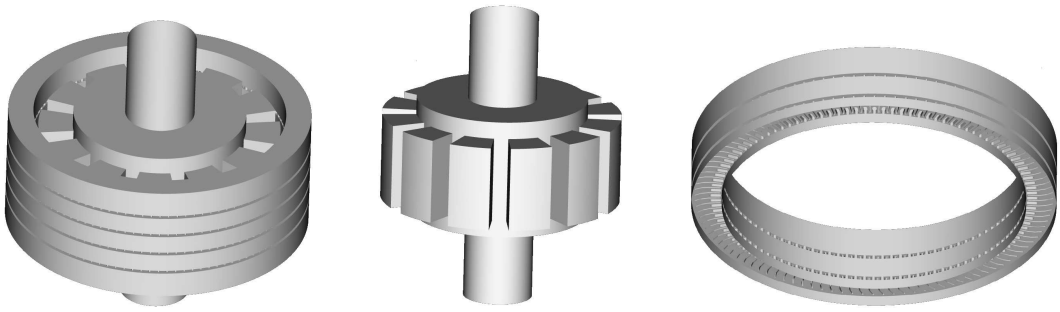

Figure 1: Simplified generator geometry used in the present work, Left: the complete model. Center: the rotor. Right: the stator with the stator channels, cut at the symmetry plane.

The stator is the outer cylindrical part of the machine, while the rotor is embraced by the stator and rotates around its axis of rotation inside the stator. The present rotor has 12 poles which induce electricity in the stator windings while rotating. The stator has a number of small cooling channels, ordered in four rows, as can be seen in figure 1. Each row contains 108 channels. Every channel is separated from the surrounding channels by

means of a thin baffle. Every coil in the stator is encompassed by a cooling channel. The heat generated by the losses in the coils and stator body should be removed from the unit to keep the machine at a suitable temperature. The aim of this work is to improve the knowledge of the air flow field within the generator and to provide a basis for future conjugate heat transfer analysis.

When the rotor rotates, the air in the space between the rotor poles and the stator builds up a pressure that drives the flow through the stator channels. A pulsating flow is generated inside each stator channel. The flow is thus very unsteady, but in the present work the simulations have been performed using the steady-state Frozen Rotor concept. This means that in the rotor region the source terms for rotation have been added to the equations. The turbulence is modeled employing the low-Re Launder-Sharma turbulence model. The use of low-Re turbulence models requires a fine mesh, in particular in the viscinity of the walls, where the first cell center should be at $y^+ \approx 5$. This way one can be sure that the boundary layer is resolved down to the viscous sublayer.

The geometry, and thus the flow within the domain, are symmetric about the center plane, so that only half of the domain needs to be considered. Furthermore, since there are 108 cooling channels in the tangential direction in each row of channels and 12 poles on the rotor, the problem can be reduced by taking into account only one pole and 9 cooling channels in each row of channels. This way, the computational domain will be much smaller (1/12 sector in the tangential direction and 1/2 in the axial direction) and cyclic boundary conditions are used on the sides of the domain. The computational domain is generated without inlets and outlets, so that the volume flow through the generator is determined by the solution, rather than by an imposed inlet volume flow. Figure 2 shows the computational domain of the base case, and a cross-section of the pole and the nine stator channels with their coils and baffles.

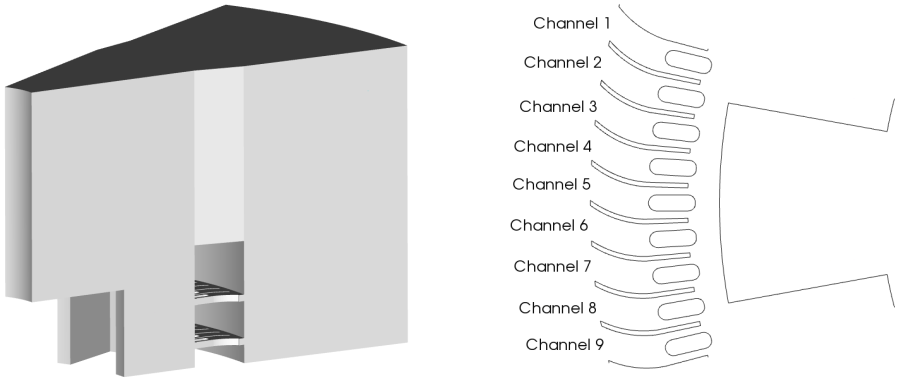

Figure 2: Left: Computational domain of the base case where the imprints of the shaft, the rotor body and one pole, as well as 1/12 of the stator can be seen. The lower boundary is a symmetry plane, the front and back boundaries are cyclic and the rest of the boundaries are walls. Right: Rotor pole and stator cooling channels. The rotor is moving clockwise when seen from above

Some of the characteristics of the generator are listed below:
- Pole diameter: $0.35m$
- Stator inner diameter: $0.365m$
- Pole radial length: $0.1m$
- Rotor rotational speed: $500rpm$
- The minimum cross-sectional area of the stator channels, near the stator coils: $\approx 8.29 \times 10^{-5}m^2$
- The total cross-sectional area between all adjacent poles, for the whole machine: $\approx 0.0393m^2$
- The total cross-sectional area for the air gap between rotor and stator, for the whole machine $\approx 0.0337m^2$

3 MATHEMATICAL MODELING AND VALIDATION

The air flow in the generator is rather complex and the velocities involved are in the turbulent flow regime. Therefore, a suitable set of mathematical equations and the discretization of those should be chosen to predict the flow. The steady-state Reynolds-averaged Navier-Stokes equations are solved using the finite volume method and the Frozen Rotor approach. A block-structured mesh is generated by the built-in blockMesh mesh generator, and m4 parametrization. The convective terms in the momentum equations are discretized using a second-order upwind scheme, while those of the turbulence equations are discretized using the first-order upwind scheme. In this work, the choice of turbulence models has been limited to steady RANS models. In order to select the best possible turbulence model to simulate the generator case a number of RANS turbulence models in OpenFOAM has been validated in the backward facing step test case. Further, to verify that OpenFOAM correctly predicts the build-up of the pressure due to the rotation, a concentric cylinder test case has been studied. These two test cases are briefly described in the following sections, followed by a brief description of the Frozen Rotor approach.

3.1 Backward Facing Step

The choice of a backward facing step as a test case was done with an intension to compare the existing turbulence models. The case study was set up as in the work by Benavides and Van Vachem[1]. A detailed study of many of the existing RANS models in OpenFOAM was performed, that is, the standard[2] $k-\varepsilon$, the realizable[3] $k-\varepsilon$, RNG[4] $k-\varepsilon$, $k-\omega$ SST[5], Launder-Sharma[6] $k-\varepsilon$, Lam-Bremhorst[7] $k-\varepsilon$, Launder-Gibson RSTM[8], Lien cubic[9] $k-\varepsilon$, Non-linear Shih[10] $k-\varepsilon$, LRR[11] and Spalart-Almaras[12]. The results were compared to each other and experiments[13]. A comparison of the velocity profiles after the backward facing step is shown in figure 3. Here, H is the height of the step and U_{cl} is the centerline velocity at the fully developed section of the inlet channel.

An important region in the domain in this case is the recirculation area after the step. As it is apparent from figure 3, the results of the Launder-Sharma $k-\varepsilon$ model are quite

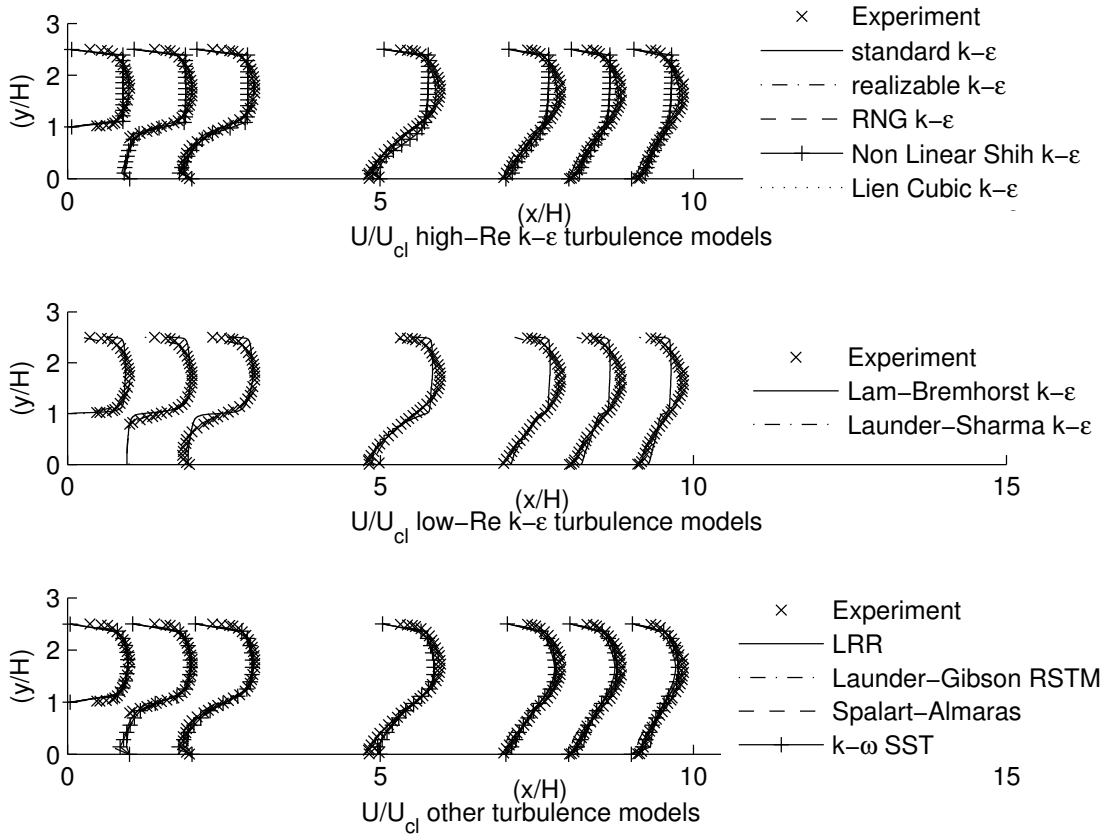

Figure 3: Comparison of the velocity profiles in the backward facing step test case

consistent with the experimental results. Therefore the Launder-Sharma $k-\varepsilon$ model was chosen to perform the simulations in the generator.

The choice of a low-Re turbulence model for performing the simulations in the generator was based on the y^+ values and resolution of the computational domain. The height of the stator channels does not allow the use of a high-Re turbulence model within an acceptable y^+ range, which would lead to a very coarse grid in the channels.

The k and ε equations in the Launder-Sharma[6] model read:

$$\frac{\partial k}{\partial t}+\frac{\partial u_j k}{\partial x_j}=\frac{\partial}{\partial x_j}\left[\left(\nu+\frac{\nu_t}{\sigma_k}\right)\frac{\partial k}{\partial x_j}\right]+\nu_t\left(\frac{\partial u_i}{\partial x_j}+\frac{\partial u_j}{\partial x_i}\right)\frac{\partial u_i}{\partial x_j}-\varepsilon \tag{1}$$

$$\frac{\partial \tilde{\varepsilon}}{\partial t}+\frac{\partial u_j \tilde{\varepsilon}}{\partial x_j}=\frac{\partial}{\partial x_j}\left[\left(\nu+\frac{\nu_t}{\sigma_\varepsilon}\right)\frac{\partial \tilde{\varepsilon}}{\partial x_j}\right]+c_{1\varepsilon}f_1\nu_t\frac{\tilde{\varepsilon}}{k}\left(\frac{\partial u_i}{\partial x_j}+\frac{\partial u_j}{\partial x_i}\right)\frac{\partial u_i}{\partial x_j}-c_{2\varepsilon}f_2\frac{\tilde{\varepsilon}^2}{k}+E \tag{2}$$

With this model, k and $\tilde{\varepsilon}$ should be set to zero at the walls. The model parameters are defined as:

$$\begin{cases} \nu_t = C_\mu f_\mu \frac{k^2}{\tilde{\varepsilon}} \\ \varepsilon = \tilde{\varepsilon} + D \\ D = 2\nu \left(\frac{\partial \sqrt{k}}{\partial x_j}\right)^2 \\ E = 2\nu\nu_t \left(\frac{\partial^2 u_j}{\partial x_j^2}\right)^2 \\ f_\mu = e^{\frac{-3.4}{(1+R_T/50)^2}} \\ f_1 = 1 \\ f_2 = 1 - 0.3e^{-R_T^2} \\ R_T = \frac{k^2}{\nu\tilde{\varepsilon}} \end{cases}$$

3.2 Concentric Cylinders

The flow in the generator is driven by the pressure build-up due to the rotation of the air in the space between the rotor poles and the stator. To verify that OpenFOAM is able to predict this behaviour correctly, a Couette flow[14] test case has been studied. Two concentric, infinitely long cylinders were modeled where the inner cylinder rotates and the outer cylinder is at rest. The theoretical pressure distribution between the inner radius, r_i, and the outer radius, r_o is given by:

$$p(r) = p(r_i) + \frac{\rho {\Omega_i}^2 {r_i}^4}{({r_o}^2 - {r_i}^2)^2} \left[\left(\frac{-{r_o}^4}{2}\frac{1}{r^2}\right) - \left(2{r_o}^2 ln\left(\frac{r}{r_i}\right)\right) + \frac{r^2}{2} + \left(\frac{{r_o}^4}{2{r_i}^2} - \frac{{r_i}^2}{2}\right) \right] \tag{3}$$

The corresponding theoretical velocity distribution reads

$$V_\theta(r) = \Omega_i r_i \frac{\frac{r_o}{r} - \frac{r}{r_o}}{\frac{r_o}{r_i} - \frac{r_i}{r_o}} \tag{4}$$

Where Ω_i is the rotational speed of the inner cylinder. The flow in the space between the two cylinders was laminar and the numerical pressure distribution and velocity profiles proved to coincide well with their corresponding theoretical curves, as shown in figure 4.

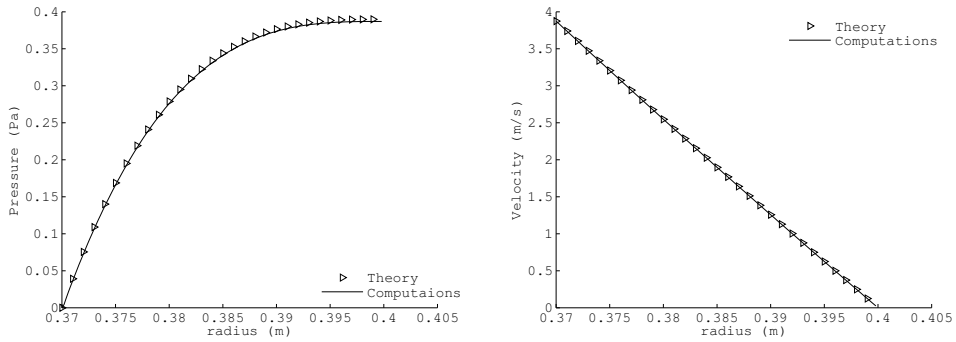

Figure 4: Comparison of the numerical and theoretical pressure distributions (left) and the velocity profiles (right) between two concentric cylinders

3.3 Frozen Rotor

The flow is simulated using the Frozen Rotor approach, which is based on a multiple reference frame method, in which an inertial region and a rotating region are specified. The two regions are separated from each other by an axi-symmetric interface[15]. The rotating region is provided with extra source terms which account for the rotation. The Navier-Stokes and continuity equations in the inertial region read

$$\nabla \cdot (\vec{u_I} \otimes \vec{u_I}) = -\nabla(p/\rho) + \nu \nabla \cdot \nabla(\vec{u_I}) \qquad (5)$$
$$\nabla \cdot \vec{u_I} = 0$$

The quantity $\vec{u_I}$ is the velocity in the inertial reference frame. The Navier-Stokes and continuity equations in the rotating part of the domain but based on convection of the absolute velocity $\vec{u_I}$ is given by

$$\nabla \cdot (\vec{u_R} \otimes \vec{u_I}) + \vec{\Omega} \times \vec{u_I} = -\nabla(p/\rho) + \nu \nabla \cdot \nabla(\vec{u_I}) \qquad (6)$$
$$\nabla \cdot \vec{u_I} = 0$$

Where $\vec{u_R}$ is the velocity in the rotating frame of reference and $\vec{\Omega}$ is the rotation vector of the rotating frame of reference.

4 GENERATOR TEST CASES

Four different designs of the generator have been investigated, a base case and three cases with geometry modifications to the base case. For all four cases the stator and pole designs, and the rotor rotational speed are kept the same. The rotor body is modified, and baffles are added, compared to the base case. The flow features have been investigated for each case, and the modifications to the geometry have then been introduced to improve the flow characteristics of the generator.

4.1 Case 1: Base Case

As can be seen in figure 5, there are no inlet and outlet boundaries included in the geometry. Instead, a region outside the stator, and above the rotor has been added. The flow thus circulates inside the closed geometry, and is driven purely by the rotation of the rotor.

4.2 Case 2: Case 1 with modified rotor body

The base case was designed with axial extensions of the rotor and stator bodies in order to provide an axial inlet. For Case 2, this extension of the rotor has been removed, while the extension of the stator is preserved, as seen in figure 5.

4.3 Case 3: Case 2 with a horizontal baffle

In this case, the geometry is modified through adding a baffle (wall of zero thickness) to the top of the stator and over the rotor of Case 2. The geometry is shown in figure 5.

4.4 Case 4: Case 3 with radial fan blade baffles

As a final modification, a fan blade baffle is added to the top of the gap between the rotor poles in Case 3. The computational domain is shown in figure 5.

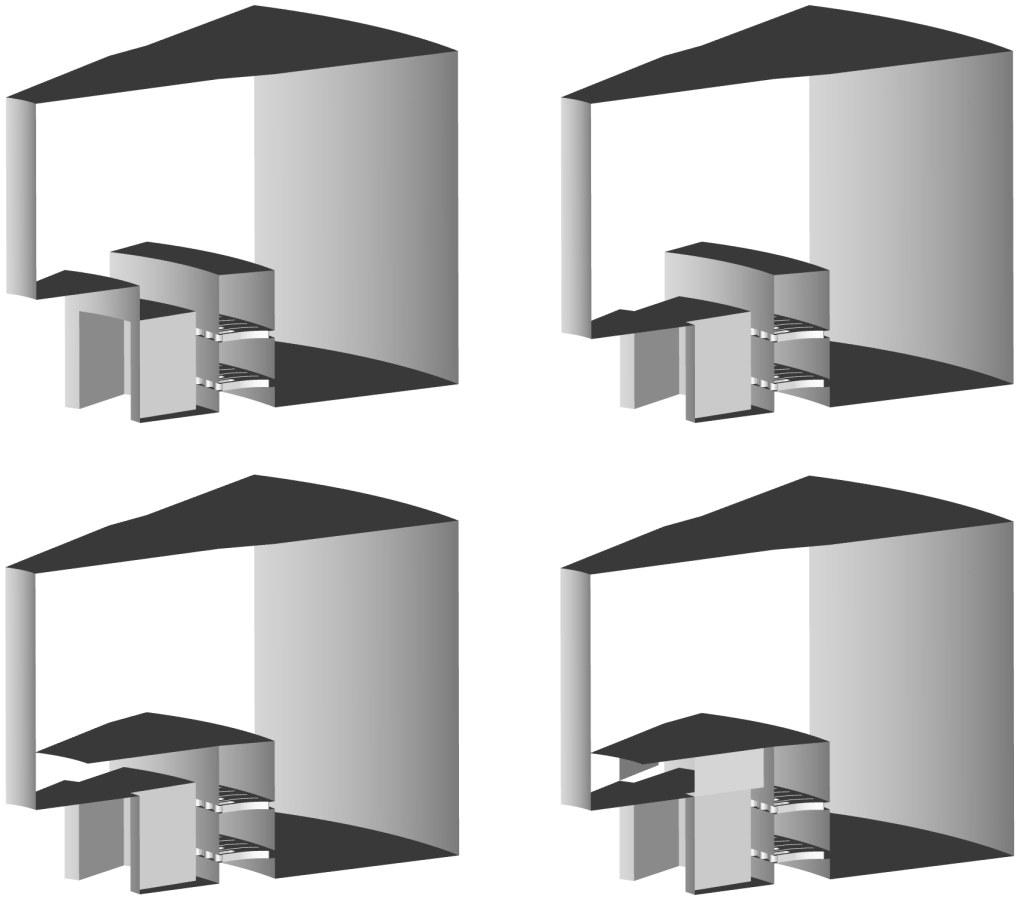

Figure 5: Geometries in the four test cases: Case 1 (top left), Case 2 (top right), Case 3 (bottom left) and Case 4 (bottom right)

The results for all test cases are described in details in the following sections.

5 RESULTS AND DISCUSSIONS

5.1 Volume Flow

The volume flow through the 18 stator channels in Case 1 is computed to $0.0029 m^3/s$. The average fluid velocity in the minimum channel cross-section area (between the stator coils and channel baffles) is thus computed to be $1.96 m/s$. The distribution of the flow in the cooling channels is shown in table 1. Since the rotation is clockwise, the rotor moves from channel 9 to channel 1. Notice that in two channels in the middle of the lower row,

the flow is negative, which means that the net flow is inwards into the rotor-stator gap, which is not desirable.

	ch 9	ch 8	ch 7	ch 6	ch 5	ch 4	ch 3	ch 2	ch 1
Upper row	8.9%	7.7%	4.7%	3.5%	3.2%	3.4%	4.4%	7.1%	8.4%
Lower row	16.5%	13.3%	0.4%	−2.3%	−0.03%	2.2%	3%	5.7%	10%

Table 1: Distribution of the volume flow through the cooling channels, Case 1

In Case 2, the volume flow through the 18 stator channels and the mean velocity in the minimum cooling channel area are $0.0027m^3/s$ and $1.70m/s$ respectively. This means that this modification to the geometry has had a negative effect on the volume flow rate, or vice versa; The design of the base case gave better flow features in the machine which was the purpose of the base case. The volume flow distribution in the cooling channels are shown in table 2. Apparently, the flow distribution in the channels is still uneven and a negative net flow rate for the channels in the middle of the lower row can still be seen.

	ch 9	ch 8	ch 7	ch 6	ch 5	ch 4	ch 3	ch 2	ch 1
Upper row	9.2%	8.8%	5.9%	4.2%	3.4%	3.3%	3.9%	6.2%	8.3%
Lower row	17.6%	12.8%	0.2%	−1.9%	−0.1%	1.9%	2%	4.9%	8.7%

Table 2: Distribution of the volume flow through the stator channels, Case 2

The baffle in Case 3 helps building up a high pressure over the pole tip which helps pushing more fluid through the machine in the axial direction and thus increases the volume flow considerably. The volume flow for the 18 stator channels in this case has been computed to $0.0079m^3/s$. This is 2.7 times the flow in Case 1. The mean velocity in the minimum cooling channel area section is $5.3m/s$. The distribution of volume flow between the stator channels in Case 3 is shown in table 3. The volume flow rates through the stator channels are in this case distributed more evenly between the channels than in Case 1. There are no channels with negative flow.

	ch 9	ch 8	ch 7	ch 6	ch 5	ch 4	ch 3	ch 2	ch 1
Upper row	6.2%	6.0%	5.7%	5.4%	5.7%	5.4%	5.3%	5.5%	5.9%
Lower row	8.3%	6.7%	4.4%	3.9%	4.2%	4.5%	4.7%	5.4%	6.7%

Table 3: Distribution of the volume flow through the stator channels, Case 3

In Case 4, the fan blades help increase the pressure build-up over the pole tip which helps pushing more fluid through the machine in the axial direction and thus increases the volume flow considerably. The volume flow through the 18 stator channels in this case has been computed to $0.017m^3/s$, which is 5.8 times that in Case 1. The mean velocity in the minimum cooling channel area section is then $11.2m/s$. The distribution of the volume flow between the stator channels in this case is shown in table 4. The distribution is much more uniform than in all other cases.

	ch 9	ch 8	ch 7	ch 6	ch 5	ch 4	ch 3	ch 2	ch 1
Upper row	5.5%	5.7%	5.9%	5.5%	4.7%	4.4%	4.5%	5.2%	5.6%
Lower row	6.0%	5.9%	5.7%	5.8%	5.9%	6.0%	5.7%	5.9%	5.9%

Table 4: Distribution of the volume flow through the stator channels, Case 4

5.2 Velocity Vectors in the Stator Channels

The velocity vectors in the center plane of the upper channel row for all cases are shown in figure 6. There is a separation where the air flow passes by the stator windings. Only in Case 4, the separated flow enters the channel behind the stator windings. The low pressure in the separation region causes a suction of the fluid from inside the channel. This means that some of the flow is going into each channel before the windings and a part of it comes out of the channel behind the winding and flows into the air gap. A large recirculation region is then generated further downstream in each channeln as shown in figure 6.

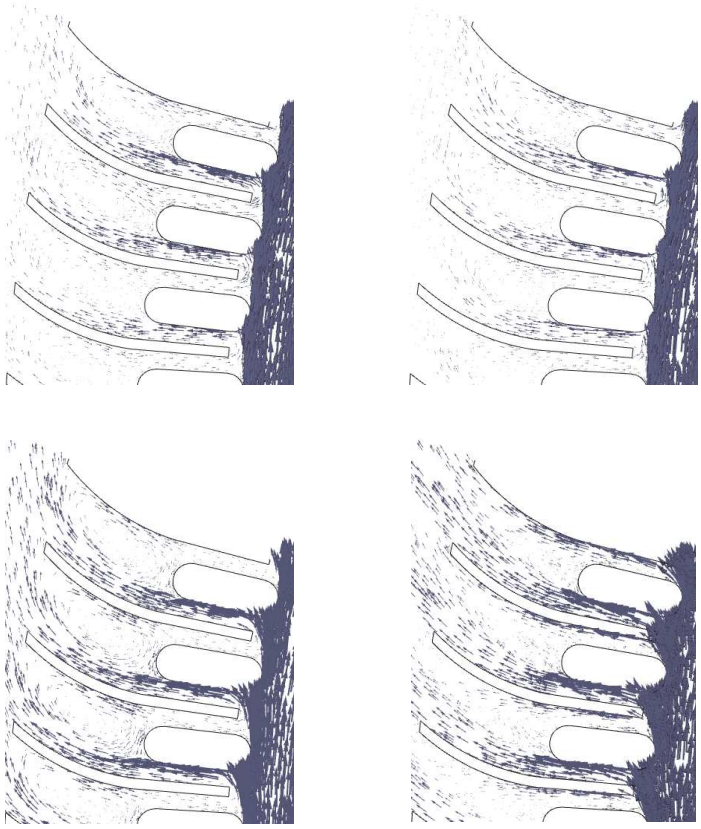

Figure 6: Velocity vectors at the center plane of the upper channel row: Case 1 (top left), Case 2 (top right), Case 3 (bottom left) and Case 4 (bottom right)

However, since the pressure in the space between the rotor and the stator in Case 4 is high enough to drive the flow from both sides of the windings into the channels, that is to say, the separation region behind the stator windings is smaller than in other cases. Further, the flow out of the stator channels is much more aligned with the baffles for Case 4.

5.3 Pressure Build-Up

Figure 7 shows the contours of relative static pressure divided by density, $((p-p_{ref})/\rho)$ $[m^2/s^2]$, in an axially-cut plane through the gap between rotor and stator. Here p_{ref} is the reference pressure at a reference cell. The reference cell is identical in all cases and is located outside the generator, on the top corner of the recirculation area where the pressure is relatively constant. As it is obvious, the pressure gradient in cases 3 and 4 are higher than in cases 1 and 2. Further, the pressure contours are more well-organized for cases 3 and 4. The largest pressure gradient is present in Case 4, which is caused by the fan blades and yields a larger suction effect and thus volume flow in this case.

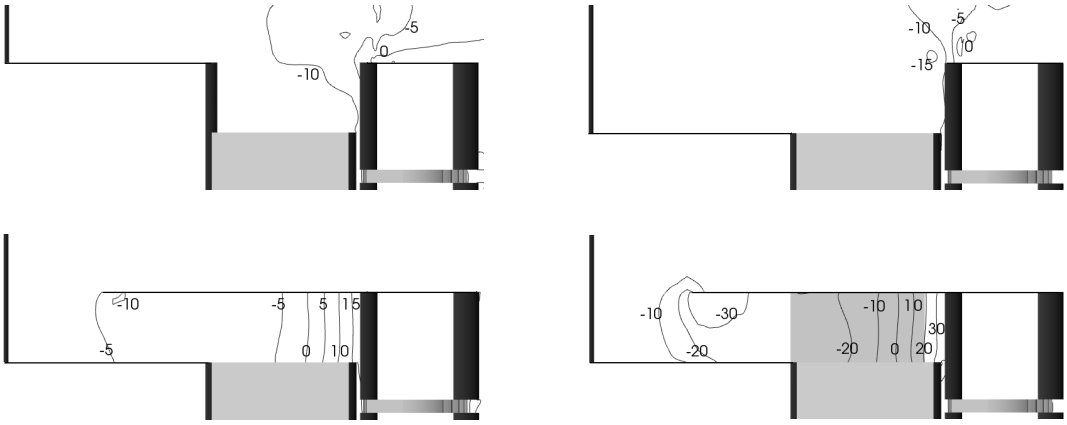

Figure 7: The pressure build-up $((p-p_{ref})/(\rho))$ $[m^2/s^2]$ in an axially cut plane through the computational domain: Case 1 (top left), Case 2 (top right), Case 3 (bottom left) and Case 4 (bottom right)

5.4 Velocity Vectors at the Inlet

The left column of figure 8 shows the velocity vectors projected on an axially cut plane through the computational domain. Here the vectors are not scaled, which means that they all have the same length and are plotted to show the flow structure. In the air gap between the rotor and the stator in cases 1 and 2, a significant part of the air flows outwards in the axial direction. This makes it impossible to specify an appropriate boundary condition in this region, and justifies the choice of a recirculating domain without inlet and outlet. The velocity contours for cases 3 and 4 show that the flow in the new inlet of the generator is purely inwards.

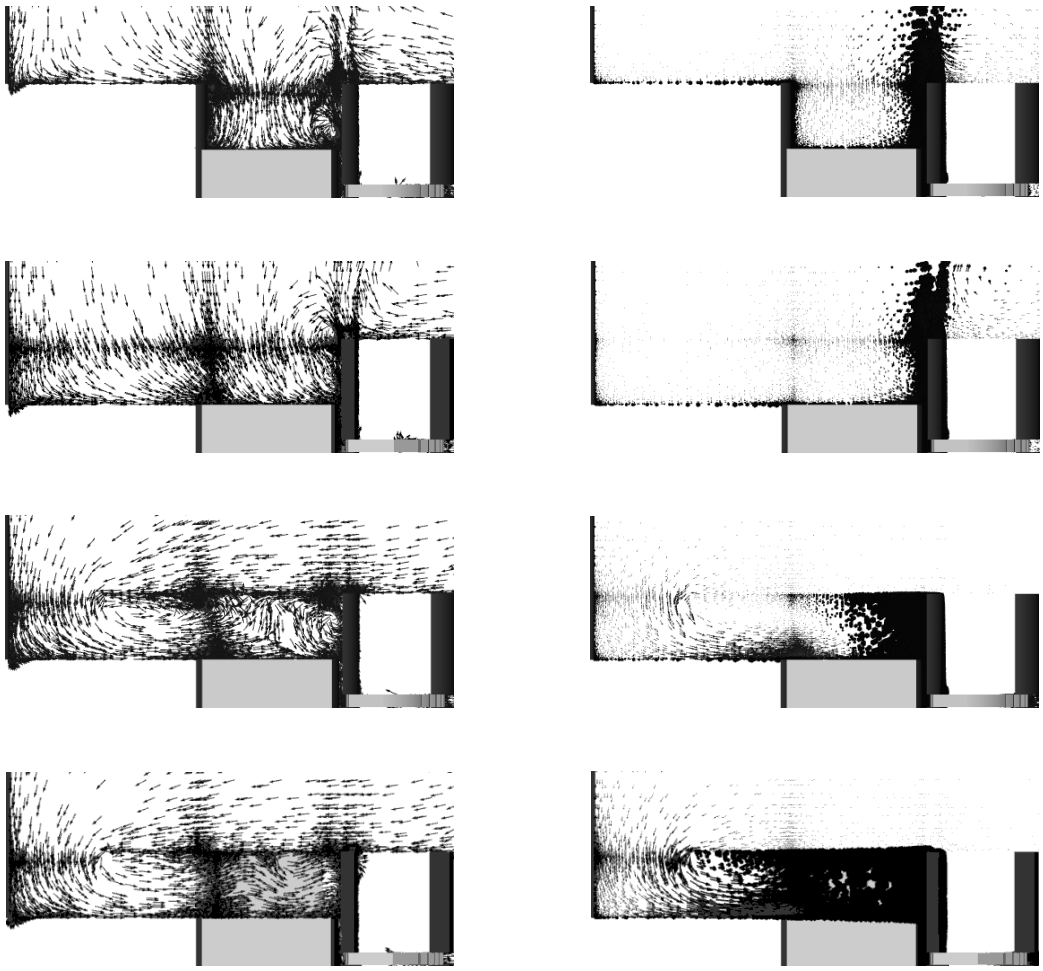

Figure 8: Velocity vectors at an axially cut plane: Case 1 (top), Case 2 (top center), Case 3 (bottom center) and Case 4 (bottom). The left column shows the unscaled velocity vectors, projected on the axial plane. The right column shows the velocity vectors in the same plane, scaled by the velocity magnitude.

The right column of figure 8 shows the velocity vectors plotted on the same axial plane. The size of each vector is scaled by its magnitude, i.e. the velocity magnitude at the corresponding point. As can be seen, in cases 3 and 4 the flow separates just at the inlet to the generator. The separation region is smaller in Case 4, compared to Case 3. This is because of larger pressure gradients, which are present in Case 4, caused by the fan blades. The larger pressure gradients cause a stronger suction, which means that the air speed is larger in Case 4, leading to a smaller separation region in that case.

5.5 Velocity Components

Figure 9 shows contour plots of the axial velocity component in a horizontally cut plane just above the rotor pole. The negative sign means that the axial velocity component is inwards. Cases 1 and 2 show larger regions with positive axial velocities, while in cases 3 and 4, a smaller region contains positive axial velocities. Furthermore, the axial velocity in the air gap between the pole and the stator is purely negative in Case 4, which yields a larger flow rate in the computational domain.

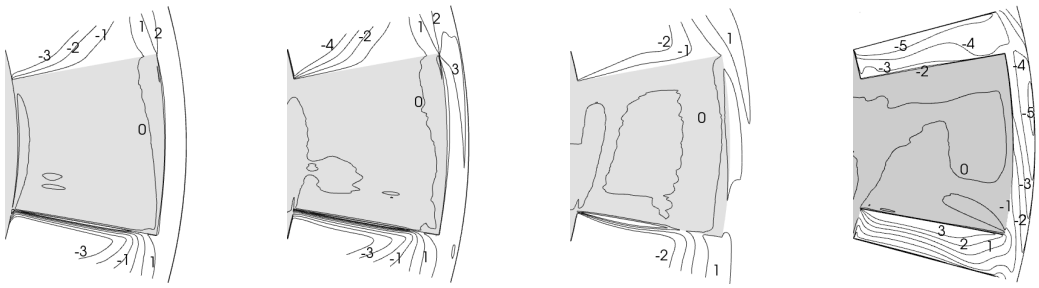

Figure 9: Axial velocity components $[m/s]$ just above the rotor pole: Case 1 (left), Case 2 (center left), Case 3 (center right) and Case 4 (right)

The radial velocity component in a horizontal plane just above the rotor pole is shown in figure 10. A negative sign means that the velocity is radially towards the axis of rotaion. Larger radial components in cases 3 and 4, compared to the cases 1 and 2 can be described by the larger pressure gradients in the former cases.

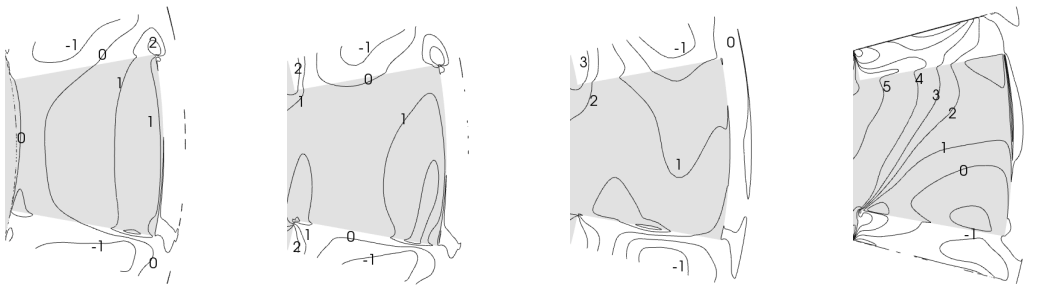

Figure 10: Radial velocity components $[m/s]$ just above the rotor pole: Case 1 (left), Case 2 (center left), Case 3 (center right) and Case 4 (right)

Figure 11 shows a comparison between the tangential velocity components in horizontally cut plane just above the rotor pole. A negative sign in this case means that the tangential velocity component is in the same direction as the rotor rotation.

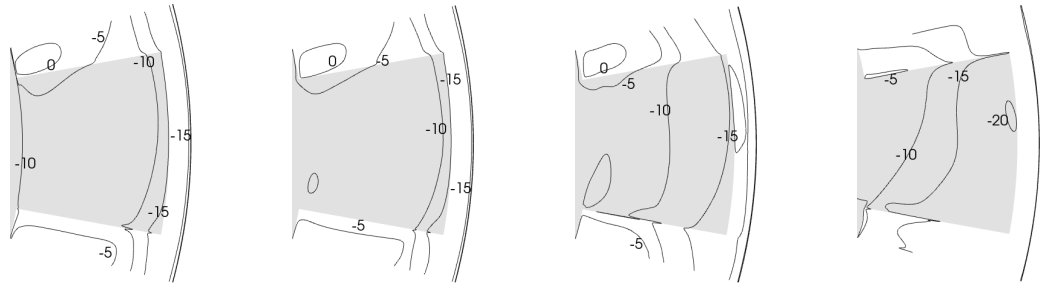

Figure 11: Tangential velocity components $[m/s]$ just above the rotor pole: Case 1 (left), Case 2 (center left), Case 3 (center right) and Case 4 (right)

6 CONCLUSIONS

Cooling is an important problem to be tackled in electric generators. Sufficient cooling in the right places will lead to higher power production efficiency and lower maintenance costs. To deal with the heat transfer phenomenon, it is important to first have a good prediction of the flow field. Four different designs of a generator have been investigated numerically. The flow rate through the machine proved to be higher when a baffle is provided on top of the stator to guide the flow axially inwards at the air gap between rotor and stator. Adding a radial fan blade on top of the space between rotor poles helps building up a pressure gradient near the stator inner radius, which increases the volume flow and makes the flow distribution between the channels more even. The numerical methodology was validated for two simple test cases, but in the future there will also be validation measurements done on a real generator.

7 ACKNOWLEDGEMENTS

The research presented was carried out as a part of "Swedish Hydropower Centre - SVC". SVC has been established by the Swedish Energy Agency, Elforsk and Svenska Kraftnät together with Luleå University of Technology, The Royal Institute of Technology, Chalmers University of Technology and Uppsala University. www.svc.nu

The computational time, hardware and facilities were provided by c^3se, center for scientific and technical computing at Chalmers University of Technology in Gothenburg Sweden and $SNIC$, Swedish National Infrastructure for Computing.

REFERENCES

[1] A. Benavides and B. van Wachem, Eulerian-Eulerian prediction of dilute turbulent gas-particle flow in a backward-facing step, *International Journal of Heat and Fluid Flow*, 2009, **30**, 452-461 (2009)

[2] F.S. Lien and M.A. Leschziner, Modeling of 3D Turbulent Flow in S-Diffuser and Transition Ducts, *2nd International Symposium Engineering Turbulence Modeling*

and Experiments, Amsterdam, The Netherlands, 1993, 217-233., (1993)

[3] T.H. Shih, W.W. Liou, A. Shabbir, Z.Yang and J.Zhu, A New k-epsilon Eddy Viscosity Model for High Reynolds Number Turbulent Flows, *National Aeronautics and Space Administration, National Technical Information Service*, Washington, DC, (1994)

[4] Y. Yakhot, S.A. Orszag, S. Thangam, T.B. Gatski and C.G.Speziale, Development of Turbulence Models for Shear Flows by a Double Expansion Technique, *Physics of Fluids* **Vol. 4**, **7**, (1992)

[5] F. Menter and T. Esch, Elements of Industrial Heat Transfer Predictions, *16th Brazilian Congress of Mechanical Engineering (COBEM)*,Uberlandia, Brazil, (2001)

[6] B. E. Launder, B. I. Sharma, (1974), Application of the Energy-Dissipation Model of Turbulence to the Calculation of Flow Near a Spinning Disc, *Letters in Heat and Mass Transfer*, **Vol. I**, **2**, 131-138 (1974).

[7] P.K. Jha and S.K. Dash, Employment of Different Turbulence Models to the Design of Optimum Steel Flows in a Tundish, *International Journal for Numerical Methods for Heat & Fluid Flow*, **Vol. 14**, **8**, (2004)

[8] M.M. Gibson and B.E. Launder, Ground Effects on Pressure Fluctuations in the Atmospheric Boundary Layer, *Journal of Fluid Mechanics*, **Vol. 86**, **86**,491-511, (1977)

[9] F.S Lien, W.L. Chen and M.A. Leschziner, Low-Reynolds-Number Eddy-Viscosity Modelling Based on Non-Linear Stress-Strain/Vorticity Relations*Engineering Turbulence Modelling and Experiments*, (1996)

[10] J. Zhu and T.H. Shih, Computation of Confined Coflow Jets With Three Turbulence Models, *International Journal for Numerical Methods in Fluids*, (1994)

[11] B.E. Launder, G.J.Reece and W. Rodi, Progress in the Development of a Reynolds-Stress Turbulence Closure, *Journal of Fluid Mechanics*, **Vol. 68**, **3**, 537-566, (1974)

[12] P. R. Spalart, S. R. and Allmaras, A One-Equation Turbulence Model for Aerodynamic Flows, *AIAA Paper 92-0439*, **1**, 5-21, (1992)

[13] J. Fessler, J. Eaton, Particle-turbulence interaction in a backward-facing step flow, Rep. MD-70, Mech. Engng Dept. Stanford University, Stanford, California (1995).

[14] F. M. White, Fluid mechanics, 6th Edition, *McGraw Hill*, (2008).

[15] O. Petit, M. Page, M. Beaudoin and H.Nilsson, The ERCOFTAC centrifugal pump OpenFOAM case-study, 3^{rd} *International Meeting of the Workgroup on Cavitation and Dynamic Problems in Hydraulic Machinery and Systems*, Brno, Czech Republic, (2009).